Infrared Physics & Technology 60 (2013) 275–280

Contents lists available at SciVerse ScienceDirect

Infrared Physics & Technology

journal homepage: www.elsevier.com/locate/infrared

Quantitative evaluation of optical lock-in and pulsed thermography for aluminum foam material

Yuxia Duan [a,b], Stefanie Huebner [c], Ulf Hassler [c], Ahmad Osman [c], Clemente Ibarra-Castanedo [b], Xavier P.V. Maldague [b,*]

[a] School of Material Science and Engineering, Beijing University of Aeronautics & Astronautics, 37, Xueyuan Road, Beijing 100191, China
[b] Computer Vision and Systems Laboratory, Department of Electrical and Computer Engineering, Université Laval, 1065, av. de la Médecine, Québec, QC G1V 0A6, Canada
[c] Fraunhofer Development Center X-ray Technologies, A Cooperative Department of IZFP Saarbrücken and IIS Erlangen, 81, Dr-Mack-Street, Fürth 90762, Germany

HIGHLIGHTS

- Probability of detection (POD) assessment.
- Pulsed and Lockin IRT approaches.
- Infrared thermographic image processing.
- Pulsed Phase Thermography (PPT).
- Thermographic Signal Reconstruction (TSR).

ARTICLE INFO

Article history:
Received 5 November 2012
Available online 10 June 2013

Keywords:
Lock-in
Pulsed
Thermography
Aluminum foam
PoD

ABSTRACT

In this article, quantitative evaluation of optical thermographic techniques relative to the non-destructive inspection of aluminum foam material is studied. For this purpose, a set of aluminum foam specimens with flat-bottom holes (FBH) was inspected by both optical lock-in thermography (LT) and pulsed thermography (PT). Probability of detection (PoD) analysis, as a quantitative method to estimate the capability and reliability of a particular inspection technique, was studied and compared for both optical LT and PT inspection results.

1. Introduction

Aluminum foam material combines the advantages of high strength and low weight. Structural efficiencies and relatively low cost makes this material of widespread use in aerospace, marine, and automotive structures [1]. Potential applications of such materials include sound and energy absorption appliances, cores for structural sandwich panels, and electromagnetic wave shields, among many others [2].

Non-destructive inspection (NDI) studies of aluminum foam material are rarely found in literature except from X-ray inspection [3,4]. The material has a low overall X-ray absorption because of the large amount of voids inside, which allows large specimens to be inspected by X-ray tomography. X-ray tomography has been proven to be a very powerful tool allowing characterizing the architecture or microstructure of cellular materials [4]. However, each NDI technique has its own strengths and weaknesses. Compared with X-ray tomography, the main advantages of optical excitation thermography are fast inspection rate, security (no harmful radiation involved) and single-side needed (stimulation and inspection on the same side) [5]. In this article, two classical optical thermographic techniques, including lock-in thermography (LT), also known as modulated thermography (MT), and pulsed thermography (PT) will be employed to inspect aluminum foam material.

Abbreviations: LT, lock-in thermography; PT, pulsed thermography; FBH, flat-bottom holes; PoD, probability of detection; NDI, non-destructive inspection; MT, modulated thermography; PPT, pulsed phase thermography; TSR, thermal signal reconstruction; PCT, principle component thermography; SVD, singular value decomposition; EOFs, empirical orthogonal functions; PCs, principal components.

* Corresponding author. Tel.: +1 418 656 2962; fax: +1 418 656 3594.
E-mail address: maldagx@gel.ulaval.ca (X.P.V. Maldague).

1350-4495
http://dx.doi.org/10.1016/j.infrared.2013.05.009

The intention of this work is to quantitatively evaluate the capability and reliability of optical LT and PT on the aluminum foam material. Probability of detection (PoD) curves, as an accepted quantitative measure of the NDI reliability and capability, are plotted to compare the obtained inspection results, by employing either LT or PT approaches.

2. Specimens and inspection configurations

2.1. Specimen description

Experimental inspections were carried out on a set of aluminum foam specimens having a total of 72 flat-bottom holes (FBH) with 12 lateral diameters D = 6, 8, 10, 12, 15, 18, 20, 22, 25, 27, 30, and 32 mm. The defect depth d, i.e. the distance between the inspected surfaces and the bottoms of the holes, goes from 1 to 6 mm.

In order to assess results, X-ray tomography was performed first for every specimen. Fig. 1a shows the schematic illustration of one aluminum foam specimen, having 5 FBH with different lateral diameters and same depth d = 2 mm. Fig. 1b and c shows the corresponding X-ray tomographic images (2D slides) of the specimen, from which we can see the 5 FBH, as well as the amount of closed cells with non-uniform sizes.

2.2. Inspection configuration

In optical excitation thermography, the energy is delivered to the surface of the specimen where the light is transformed into heat; while an infrared camera is used to monitor changes of the object's surface temperature. Since the subsurface discontinuities may alter the diffusion of the heat, this will affect the cooling behavior of the nearby region on the surface.

In this study, the optical thermography inspection setup included two OMNILUX PAR64 (1000 W) halogen lamps, which generated sinusoidal or pulsed thermal waves. The lamps and the infrared camera were located on the same side with respect to the specimen surface, as shown in Fig. 2. A CEDIP titanium infrared camera was used to detect the thermal wave. Table 1 shows the important technical specifications of the CEDIP camera.

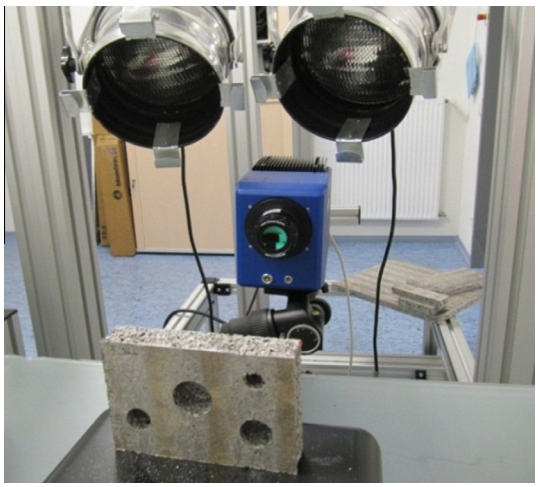

Fig. 2. Photograph of the optical thermography system.

Table 1
Technical specification of CEDIP titanium camera.

Technical specification	Explanation/value
Sensor type	MCT
Waveband	3.7–4.5 μm
Pixel resolution	640 × 512
Pixel raster	15 μm
Thermal sensitivity	<18 mK
Cooler	Integrated stirling cooler
Max full frame rate	117 Hz
Digital output	14 Bit GigE
Integration time	10 μs–5 ms
Temperature calibration	0–160 °C

2.2.1. Lock-in thermography

In optical LT, the absorption of modulated optical radiation results in a temperature modulation that propagates as a thermal wave into the inspected component. As the thermal wave is reflected at the defect boundary, its superposition to the original thermal wave causes changes in amplitude and phase of the

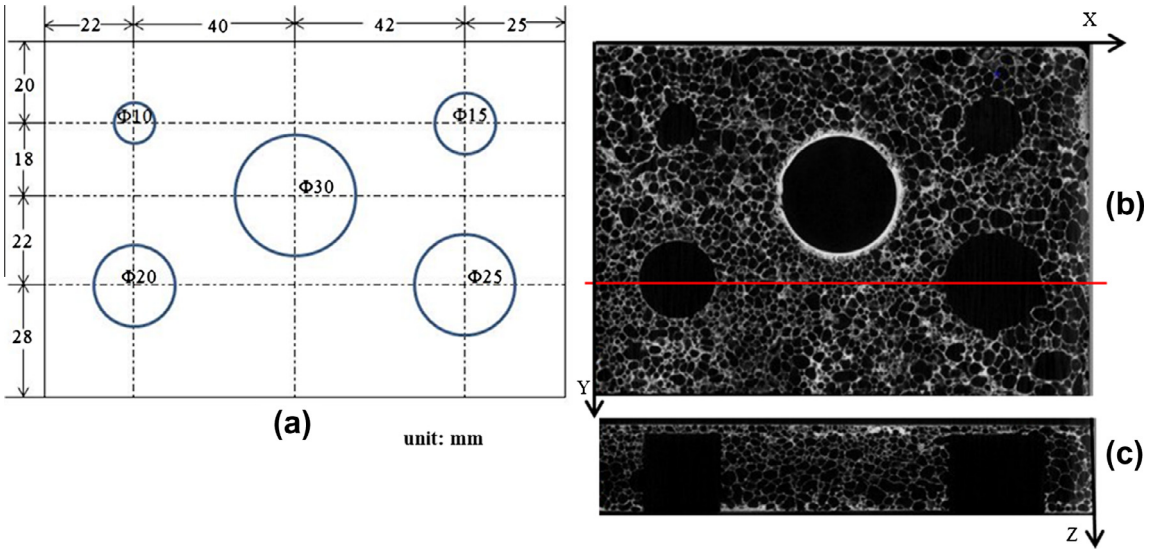

Fig. 1. (a) Schematic illustration of one representative specimen with defect depth d = 2 mm, (b) X–Y slide tomographic image (Z = 3 mm), and (c) X–Z slide tomographic image of the marked horizontal line.

response signal at the surface, which are recorded at the same time using an infrared camera [6].

From the Fourier's Law one-dimensional solution for a periodic thermal wave propagating through a semi-infinite homogeneous material, the thermal wave diffusion length is given by [7]:

$$\mu = \sqrt{\frac{2\alpha}{\omega}} = \sqrt{\frac{\alpha}{\pi \cdot f}} \tag{1}$$

where $\alpha = \kappa/\rho c_p$ is the diffusivity of material, with κ being the thermal conductivity, ρ the density, c_P the specific heat (at constant pressure); and $\omega = 2\pi f$ is the modulation frequency. The probing depth z, for amplitude images, is given by the thermal diffusion length equation $z \sim \mu$ [8], see Eq. (1). For the phase, reported values range from 1.5μ [9] to more than 2μ [8]. From Eq. (1), it is clear that probing depth heavily depends on the heating frequency; the lower modulation frequency, the deeper penetration.

Generally, inspections start at a relatively high excitation frequency at which, depending on the thermal diffusivity of the material, only shallow defects are visible. In order to detect deeper defects, the excitation frequency is gradually decreased until the appropriate value is reached. Preliminary tests indicated that excitation frequencies ranging from 1 down to 0.05 Hz were adequate to completely cover the depth range of interest, from very shallow to 6 mm. The acquisition frame rate was set to 50 Hz. Longer acquisition times are required for the low frequencies to obtain sufficient modulating periods with which to average. Increasing the number of periods aided in reducing the noise level and to improve image signal-to-noise ratio (SNR) and subsequently, defect contrast.

Phase images or phasegrams are usually preferred for analysis since they are more tolerant to the non-uniform heating, emissivity variations, and environmental reflections compared to amplitude images [10]. Furthermore, as discussed above, they provide probing capabilities deeper than amplitude images.

One commonly used method to retrieve phase and amplitude is 4-point methodology for sinusoidal stimulation phase [11,12]. The 4-point methodology is fast but it is valid only for sinusoidal stimulation and is affected by noise. The signal can be de-noised in part by averaging several points instead of a single one and/or by increasing the number of cycles. Another possibility is to fit the experimental data using least squares regression [13] and to use this synthetic data to calculate the amplitude and the phase. These two alternatives however contribute to slow down the calculations. Alternatively, the Fourier Transform (FT) can be used to extract amplitude and phase information from LT data. The FT can be used with any waveform (even transient signals as in pulsed thermography, see below) and has the advantage of de-noising the signal. In this article, FT is employed to retrieve phasegram from the raw images.

2.2.2. Pulsed thermography

In optical PT, the specimen surface is submitted to a short heating pulse using a high power optical source. The duration of the pulse may vary from a few milliseconds (~2–15 ms using flashes) to several seconds (using lamps) [14]. Absorption of the short time pulse energy elevates the specimen surface temperature. As time elapses and heating pulse vanishes, the surface temperature will decrease uniformly for a piece without internal flaws. On the contrary, subsurface discontinuities will change the diffusion of heat flow and produce abnormal temperature patterns at the surface that can be detected with an IR camera [15]. In this study, two OMNILUX PAR64 (1000 W) halogen lamps were employed to generate 0.5 s long pulse energy.

Data acquisition in PT is fast and allows the inspection of extended surfaces. However, raw PT data is difficult to handle and analyze because of non-uniform heating and reflections. Contrary to LT, there are a great variety of processing techniques that have been developed to improve the inspection results. In this article, data processing methods that will be used in PT includes:

- Pulsed phase thermography (PPT) [16], which allows retrieving phase and amplitude data from a PT experience. This method can be thought as being a combination of PT and LT. In a similar manner as for LT, phase data is commonly analyzed since it is more tolerant to the non-uniform heating and environmental reflections.
- Thermographic signal reconstruction (TSR) [17], which provides a significant degree of data compression since only polynomial coefficients are stored. It is also convenient for generating derivative images without additional noise contributions. Furthermore, performing 1st or 2nd time derivatives of the TSR provides a significant improvement in signal to noise performance as well as providing a good sensitivity to smaller and deeper defects [18].
- Principal component thermography (PCT) [19], which uses singular value decomposition (SVD) to extract the spatial information described by empirical orthogonal functions (EOFs) and temporal information represented by principal components (PCs) from a thermogram sequence. This method usually results in high levels of thermal contrast for the subsurface defect.

In order to obtain the optimum results, two important parameters need to be carefully selected: the sampling rate f_s, and the acquisition time t_{acq} [14]. In this work, the acquisition time t_{acq} ranged from 20 to 60 s, while the sampling rate f_s varied from 25 to100 Hz, depending on the depths of the flat-bottom holes.

3. Result images analysis

All of 12 aluminum foam specimens were inspected by the same lab inspector. For LT data, phasegrams were analyzed by an experienced inspector. For PT data, FFT, time derivatives of TSR, and PCT data processing techniques were carried out to improve the defect detection capability by the same experienced inspector. Results images from LT and PT inspection, relative to a specimen with defects of different sizes but the same depth (2 mm), are shown in Fig. 3.

The inspector visually examined the result images to give a qualitative evaluation of the appearance of every defect. It should be noted that the inspector knows the real location of every defect, which may influence the inspector's interpretation. The inspector record the inspection result in terms of whether or not a flaw was found: 1 denotes a flaw was found, 0 denotes a flaw was not found. Subsequently, a set of hit/miss data was obtained, which will be used for the following statistical analysis to obtain the probability of detection (PoD) curves. Table 2 shows a summary of the LT and PT inspection results.

4. Probability of Detection (PoD) analysis and comparison

PoD curves are the generally accepted method for characterizing and quantifying non-destructive inspection capability and reliability [20]. A POD curve given as a function of a flaw characteristic, such as the size of flaw, is usually estimated from data taken from inspections. As we know, defect depth significantly influences the inspection result as well as the defect size detected in thermographic technique. Hence, the PoD curves as a function of aspect ratio r (D/d) were studied. The PoD function can be formulated either by the quantitative response data or the hit/miss data (also called binary data). In this article, data is organized as hit/miss

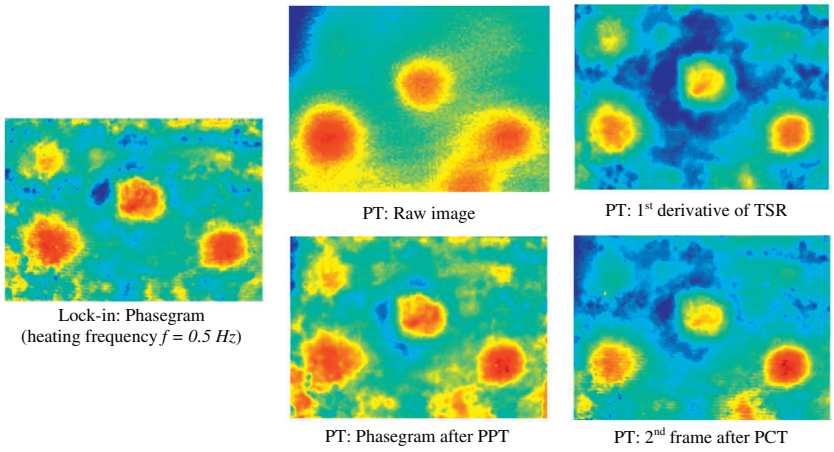

Fig. 3. Results images obtained from LT and PT, relative to a specimen with defects of different size but the same depth 2 mm.

Table 2
Summary of LT and PT inspection results.

Inspection techniques	Results images	Number of FBH detected	Detection rate (%)
LT	Phasegrams	46	64
PT	Raw images	40	55
PT	PPT phasegrams	44	61
PT	TSR 1st time derivative images	50	69
PT	PCT EOFs	44	61

data, i.e. inspection result is recorded as either detected (=1) or not (=0) for every defect aspect ratio.

The first step for PoD analysis of hit/miss (binary) data is choosing the model. There are four models corresponding to four link functions (also called transform function) [21]. The log-odds and log-normal models are commonly used in practice, especially for symmetric data sets. The earliest form of log-odd model is given by [20]:

$$\mathrm{PoD}(a) = \frac{\exp(\alpha + \beta \ln a)}{1 + \exp(\alpha + \beta \ln a)} \tag{2}$$

A mathematically equivalent form of log-odds PoD model is given by [20]:

$$\mathrm{PoD}(a) = \left\{1 + \exp - \left[\frac{\pi}{\sqrt{3}}\left(\frac{\ln a - \mu}{\sigma}\right)\right]\right\}^{-1} \tag{3}$$

The parameters of Eqs. (1) and (3) are related by [20]:

$$\mu = \frac{-\alpha}{\beta} \tag{4}$$

$$\sigma = \frac{\pi}{\sqrt{3}\beta} \tag{5}$$

The log-odds PoD function is practically equivalent to a cumulative log-normal distribution $\Phi()$ with the same parameters μ and σ of Eq. (3) [20,22,23].

For quantitative response data, the random error between the observed responses and the model predictions has a continuous, Gaussian (normal) distribution. However, for hit/miss data, the random error between outcomes and model predictions is decidedly non-normal (it's binomial) and so treating it as Gaussian and implementing ordinary regression would produce inaccurate and unreliable parameter estimates. In this study, iteratively reweighted least-squares, a special maximum likelihood method was implemented to obtain the estimate parameters: intercept α and slope β. From Eqs. (4) and (5), cumulative log-normal distribution $\Phi()$ with the parameters μ and σ will be determined.

For the models being used in NDT reliability studies, the maximum likelihood estimated parameters are asymptotically joint normal distribution with means given by the true parameter values, θ_i, and the variance–covariance matrix defined by [20]:

$$V = I^T \tag{6}$$

where I is the information matrix whose elements I_{ij} are the expected (E) values [20]:

$$I_{ij} = -E\left[\frac{\partial^2}{\partial\theta_i \partial\theta_j} \log f(X_i;\theta)\right], \quad i,j = 1,\ldots,k \tag{7}$$

In application, the maximum likelihood estimate $\hat{\theta}$ is substituted for θ in Eq. (7). A procedure developed by Cheng and Iles can be used to place lower confidence bounds on the PoD(a) function [24,25]. Such bounds are calculated from the variance–covariance matrix of the estimates and reflect the sensitivity of the experiment to both the number and sizes of flaws in the experimental specimens. The assumed PoD(a) model is a cumulative log-normal distribution function with parameters $\theta = (\mu, \sigma)'$. For distribution functions defined by location and scale parameters (as is the case of the log-normal distribution), the information matrix I can be written in the form:

$$I(\mu,\sigma) = \frac{n}{\sigma^2}\begin{bmatrix} k_0 & -k_1 \\ -k_1 & k_2 \end{bmatrix} \tag{8}$$

where n is the number of defects in the experiment. The lower one-sided confidence bound of the PoD(a) function is given by:

$$\mathrm{POD}_{\alpha}(a) = \Phi(\hat{z} - h) \tag{9}$$

where (z) is the standard cumulative normal distribution, α denotes the confidence level and:

$$\hat{z} = \frac{\log(a) - \hat{\mu}}{\hat{\sigma}} \tag{10}$$

$$h = \left\{\frac{\gamma}{nk_0}\left[1 + \frac{(k_0\hat{z} + k_1)^2}{k_0k_2 - k_1^2}\right]\right\}^{0.5} \tag{11}$$

where n is the number of defects in the experiment, γ is obtained from Table 3 for the number of defects in the experiment.

Commonly, the $a_{90/95}$ magnitudes, i.e. the size of the flaw for which the 95% lower confidence bound crosses the 90% PoD level, will be determined. It is guaranteed that flaws with the size of $a_{90/95}$ will be detected with 90% probability where only 5% might fall outside this confidence limit in case the experiment is repeated.

Table 3
Value of γ for lower confidence bounds on the PoD(a) function [20].

Sample size	20	25	30	40	50	60	80	100	∞
Confidence level (%)									
90	3.903	3.884	3.871	3.855	3.846	3.839	3.831	3.827	3.808
95	5.243	5.222	5.208	5.191	5.180	5.173	5.165	5.159	5.138
99	8.401	8.376	8.359	8.338	8.325	8.317	8.306	8.300	8.273

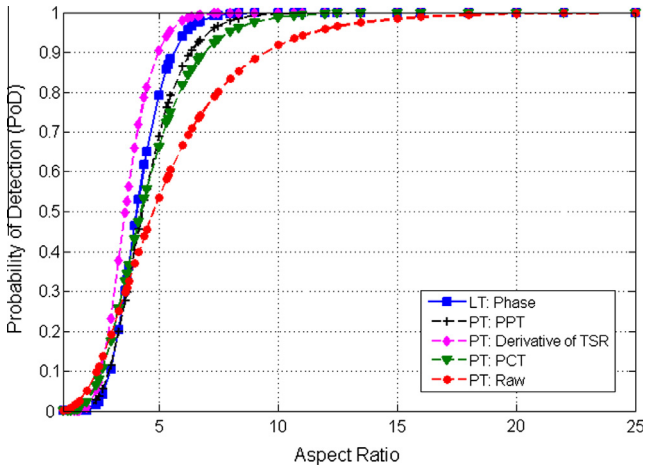

Fig. 4. PoD curves of LT and PT with different data processing manipulations, including raw data.

Table 4
r_{90} and $r_{90/95}$ values obtained by LT and PT.

Inspection techniques	Result images	r_{90}	$r_{90/95}$
LT	Phasegrams	5.5	7.1
PT	Raw images	9.1	14.5
PT	PPT phasegrams	6.2	8.3
PT	TSR 1st time derivative images	4.9	6.3
PT	PCT EOFs	6.7	9.4

Except the methodology described above, which is suggested in Metals Handbook [20], another methodology that uses likelihood ratio statistic to define the confidence region can also be found in literature [26,27].

Fig. 4 compares the PoD curves of LT and PT. The effects of commonly used data processing methods in PT, including PPT, derivative of TSR, and PCT are compared as well.

Lower confidence bounds at 95% were calculated for each data set to reflect the degree of uncertainty. Table 4 shows the defect aspect ratio with 90% PoD (r_{90}) and the defect aspect ratio for which 90% PoD is reached at 95% confidence level ($r_{90/95}$).

As can be seen form Table 4, the inspection capability of LT is higher than PT without additional processing of raw data, i.e. the r_{90} and $r_{90/95}$ values are lower. However, the inspection results of PT were dramatically improved after data processing. The inspection capability of PT is even higher than the LT after 1st time derivative of TSR processing.

5. Conclusion

Optical excitation thermography is an attractive tool for the non-destructive evaluation of aluminum foam material, especially in the cases where X-ray tomography may not available, such as inspections of very large areas, accessibility restricted to one side of the sample.

The main advantages of LT are that the directly acquired data is rather easy to handle. However, long inspection time constitutes the principal drawback of LT, since a single experiment should be carried out for every inspected depth. An alternative is to use a very low stimulation frequency, but this approach will only work for FBH, which are thick defects ranging from the initial depth to the total thickness of the sample. In the case of delaminations for instance, several defects would be missing using a very low modulating frequency. Data acquisition in PT is relatively fast. However, raw PT data is commonly difficult to analyze because of the non-uniform heating or reflections. As a result, additional processing of the data is required.

PoD analysis results of LT and PT indicate that post-processing in PT, including PPT, TSR and PCT, improved the thermal contrast for the subsurface defect, especially the smaller and deeper defects. As a result, PT and LT provide comparable inspection results.

Acknowledgements

Authors wish to thank to Entwicklungszentrum Röntgentechnik (EZRT), Fraunhofer IIS, Fürth, Germany for providing the specimen processing, X-ray tomography results and infrared thermography system. The Ministère des Relations Internationales du Québec: Programme de coopération scientifique Québec-Bavière and NSERC are acknowledged as well for their support.

References

[1] Y. Feng, H. Zheng, Z. Zhu, F. Zu, The microstructure and electrical conductivity of aluminum alloy foams, Materials Chemistry and Physics 78 (1) (2003) 196–201.
[2] A. Paul, U. Ramamurty, Strain rate sensitivity of a closed-cell aluminum foam, Materials Science and Engineering: A 281 (1–2) (2000) 1–7.
[3] J. Banhart, H. Stanzick, L. Helfen, T. Baumbach, K. Nijhof, Real-time X-ray investigation of aluminium foam sandwich production, Advanced Engineering Materials 3 (6) (2001) 407–411.
[4] E. Maire, A. Fazekas, L. Salvo, R. Dendievel, S. Youssef, P. Cloetens, J.M. Letang, X-ray tomography applied to the characterization of cellular materials. Related finite element modeling problems, Composites Science and Technology 63 (2003) 2431–2443.
[5] X. Maldague, Introduction to NDT by active infrared thermography, Materials Evaluation 6 (9) (2002) 1060–1073.
[6] A. Gleiter, C. Spießberger, G. Busse, Lockin-thermography with optical or ultrasound excitation, in: 10th International Conference of the Slovenian Society for Non-Destructive Testing, Ljubljana, Slovenia, 1–3 September, 2009.
[7] G. Giorleo, C. Meola, Comparison between pulsed and modulated thermography in glass–epoxy laminates, NDT & E International 35 (5) (2002) 287–292.
[8] G. Busse, A. Rosencwaig, Subsurface imaging with photoacoustics, Applied Physics Letters 36 (1980) 815–816.
[9] R.L. Thomas, J.J. Pouch, Y.H. Wong, L.D. Favro, P.K. Kuo, A. Rosencwaig, Subsurface flaw detection in metals by photoacustic microscopy, Journal of Applied Physics 51 (1980) 1152–1156.
[10] X.P.V. Maldague, Theory and Practice of Infrared Technology for Nondestructive Testing, Wiley-Interscience, New York, 2001.
[11] D. Wu, G. Busse, Lock-in thermography for nonDestructive evaluation of materials, Revue Générale de Thermique 37 (1998) 693–703.
[12] G. Busse, D. Wu, W. Karpen, Thermal wave imaging with phase sensitive modulated thermography, Journal of Applied Physics 71 (1992) 3962–3965.
[13] J.C. Krapez, Compared performances of four algorithms used for modulation thermography, in: 4th Conference on Quantitative InfraRed Thermography – QIRT, Eurotherm Seminar 60, Lodz, Pologne, 1998.
[14] C. Ibarra-Castanedo, Quantitative Subsurface Defect Evaluation by Pulsed Phase Thermography: depth Retrieval With the Phase, Ph.D. thesis, Université Laval, 2005.

[15] C. Ibarra-Castanedo, M. Genest, S. Guibert, J.-M. Piau, X.P.V. Maldague, A. Bendada, Inspection of aerospace materials by pulsed thermography, lock-in thermography and vibrothermography: a comparative study, Proceedings of SPIE 6541 (2007) 654116.1–654116.9.
[16] X. Maldague, S. Marinetti, Pulse phase infrared thermography, Journal of Applied Physics 76 (5) (1996) 2694.
[17] S.M. Shepard, J.R. Lhota, B.A. Rubadeux, D. Wang, T. Ahmed, Reconstruction and enhancement of active thermographic image sequences, Optical Engineering 42 (5) (2003) 1337–1342.
[18] S.M. Shepard, T. Ahmed, B.A. Rubadeux, D. Wang, J.R. Lhota, Synthetic processing of pulsed thermographic data for inspection of turbine components, Insight 43 (2001) 587–589.
[19] N. Rajic, Principal component thermography for flaw contrast enhancement and flaw depth characterization in composite structures, Composite Structure 58 (2002) 521–528.
[20] A.P. Berens, NDE reliability data analysis, Metals Handbook, 9th ed., vol. 17, ASM International, Ohio, 1989.
[21] US Air Force Aeronautical Systems Center, Non-destructive Evaluation System Reliability Assessment, in: Military Handbook, 2009.
[22] D.S. Forsyth, A. Fahr, An evaluation of probability of detection statistics, in: Airframe Inspection Reliability under Field/Depot Conditions, Neuilly-sur-Seine Cedex, France, November, 1998.
[23] Y. Duan, P. Servais, M. Genest, C. Ibarra-Castanedo, X. Maldague, ThermoPoD: a reliability study on active infrared thermography for the inspection of composite materials, Journal of Mechanical Science and Technology 26 (7) (2012) 1985–1991.
[24] R.C.H. Cheng, T.C. Iles, Confidence bands for cumulative distribution functions of continuous random variables, Technometrics 25 (1983) 77–86.
[25] R.C.H. Cheng, T.C. Iles, One sided confidence bands for cumulative distribution functions", Technometrics 32 (1988) 155–159.
[26] S.W. Floyd, The calculation and use of confidence bounds in POD models, Review of Quantitative Nondestructive Evaluation 26 (2007).
[27] W.Q. Meeker, L.A. Escobar, Teaching about approximate confidence regions based on maximum likelihood estimation, The American Statistician 49 (1995).